Sensors and Materials, Vol. 36, No. 8 (2024) 3313–3333
MYU Tokyo

S & M 3734

Cross-link Interference Mitigation Method for Heterogeneous Frame Structures of 5G-Advanced Network

Jianbin Wang, Jing Jin, Haiyun Zhu,* and Song Wu**

China Telecom Corporation Limited Zhejiang Branch, Hangzhou 310005, P.R. China

(Received February 9, 2024; accepted April 3, 2024)

Keywords: heterogeneous frame structure, cross-link interference, slot level AMC scheduling, interference mitigation algorithm, adaptive slot turn-off, edge user adaptive scheduling

To address the challenges posed by the diverse demands of mobile users and vertical industries, it is crucial for 5G-advanced (5G-A) networks to exhibit flexibility in system design across both the physical and higher layers. A single-frame structure alone cannot provide the necessary flexibility to accommodate multiple traffic modes. Therefore, we investigate a heterogeneous frame structure that meets the requirements. However, this structure will cause severe cross-link interference (CLI) and degrade the performance. To solve this problem, four CLI mitigation methods are proposed: slot level adaptive modulation and coding (AMC) scheduling (method 1), interference mitigation algorithm (method 2), adaptive slot turn-off (method 3), and edge user adaptive scheduling (method 4). The experimental results show that the CLI problem can be completely mitigated by deployed method 3 in a macro-base station (BS) with a low load scenario, the micro-BS uplink (UL) throughput was improved by 75.8%. Otherwise, with macro-BS in the high load scenario, when method 4 was implemented in macro-BS and methods 1 and 2 were deployed in micro-BS, a nearly complete CLI mitigation effect was obtained, reflecting that the micro-BS UL throughput increased to 57.4%. These methods are elaborated upon and evaluated within practical 5G-A networks, and the experimental results not only demonstrate the viability and efficacy of the above methods but also highlight their potential applications in future usage scenarios.

1. Introduction

With the deployment of the Internet of Things (IoT), the quantity of devices is increasing rapidly, and the data traffic is experiencing an explosive increase.[1,2] These impose rigorous high requirements on next-generation networks, such as the large bandwidth, high data rate, and low latency.[3] To meet the demands of future networks, various technologies have been introduced. Some new technologies are aimed at enhancing the spectral efficiency and data rate. The introduction of the mmWave can expand the spectral range.[4] Multiple-input multiple-output (MIMO) can lead to transmission and reception diversity.[5] In addition, spectral utilization can also be improved by flexible and dynamic duplex operations.[6]

*Corresponding author: e-mail: zhuhy.zj@chinatelecom.cn
**Corresponding author: e-mail: wus17@chinatelecom.cn
https://doi.org/10.18494/SAM5022

ISSN 0914-4935

Among these different technologies, the duplex modes can achieve efficient spectral utilization and provide a higher quality, and have seen widespread application in both 4G and 5G networks.[7] Currently, a duplex mode comprises a frequency division duplex (FDD) and a time division duplex (TDD). In the FDD mode, downlink (DL) and UL operate on distinct frequency bands. The FDD spectrum mandates multiple bands, with one band dedicated to UL and another to DL. On the other hand, in TDD, both UL and DL work within the same band but utilize different time slots.[8] To expand the range of TDD, new bands for TDD have been introduced in 5G New Radio (5G-NR).[9] In addition, dynamic TDD was also introduced to improve the performance by gaining duplex flexibility.[10] Different from the traditional static TDD mode, dynamic TDD can adaptively schedule UL and DL traffic on the basis of the traffic scenario; this can minimize latency and enhance the efficiency of time resource utilization.

5G public network resources are mainly based on a large DL resource 7D3U (7 DL time slots including the S slot that is 3 UL time slots) frame structure, with a peak UL throughput of around 280 Mbps. 5G vertical industries mainly rely on the demand for large UL resources (such as video surveillance and backhaul networks). Traditional mobile communication systems adopt a unified 7D3U frame structure for a large DL resource, but are prone to UL limitations, making it difficult to meet the communication business needs of different scenarios. As seen in the right-hand illustration of Fig. 1(a), the 1D3U (actually, there are 4 DL slots including the S slot, and 6 UL slots) frame structure configuration can effectively solve the problem of a limited UL capacity, with a peak UL throughput of around 600 Mbps, and the 7D3U and 1D3U frame structures jointly form heterogeneous networks, as seen in Fig. 1(a).

The main challenge of the heterogeneous TDD network is the cross-link interference (CLI) problem.[11] CLI refers to the interference that occurs in TDD systems when adjacent cells communicate in the same frequency band using different time slots. In TDD systems, communication alternates between DL and UL in the same frequency band, and CLI arises when the UL time slot of one base station (BS) interferes with the DL time slot of an adjacent BS. This interference typically occurs in areas where the time slots of adjacent cells overlap,

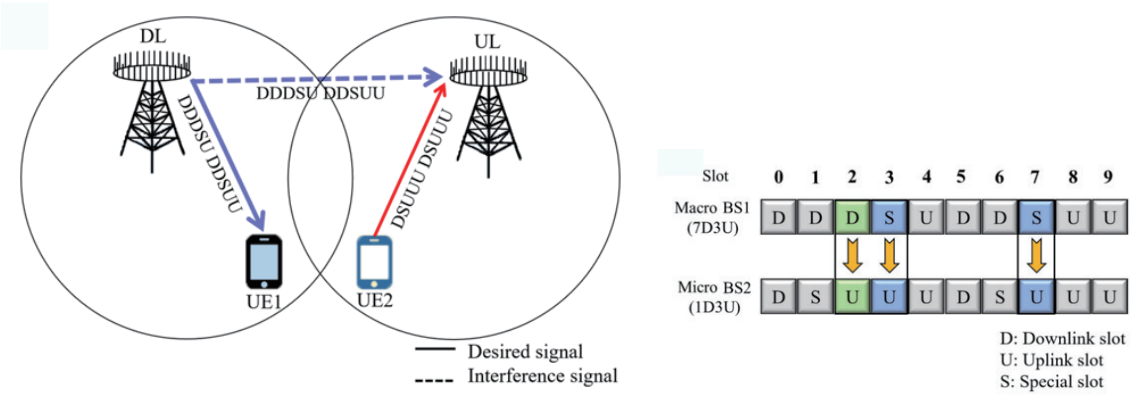

(a) (b)

Fig. 1. (Color online) (a) 7D3U and 1D3U slot configurations of heterogeneous network. (b) Cross-link interference occurring in slots 2, 3, and 7 of heterogeneous network.

causing simultaneous UL and DL communication and potential interference between DL and UL signals. For example, the CLI problem occurs in slots 2, 3, and 7 of the heterogeneous network, as seen in Fig. 1(b). CLI is a significant challenge in TDD systems, especially in high-density and high-capacity networks such as 5G, where flexible slot planning between different cells is essential to accommodate diverse services and traffic demands. Effectively addressing CLI is crucial for enhancing the overall system performance and improving user experience. The research and implementation of various interference mitigation techniques play a key role in tackling this challenge.

Nowadays, CLI mitigation schemes are attracting the interest of many researchers, and the main works focus on coordination-based schemes. The main idea of the solution is to avoid CLI in advance.[12] Clustering is an effective method of avoiding CLI. Xin *et al.*[13] proposed an innovate opportunistic interference mitigation (OIM) architecture that enhances dynamic TDD in ultradense networks (UDNs) by leveraging multi-user diversity and interference-aware transmission. Yu *et al.*[14] designed a clustering scheme to group remote radio heads (RRHs) into different sets and proposed a dynamic resource allocation solution for heterogeneous cloud radio access networks. Some researchers focus on scheduling and resource allocation to avoid CLI. Razlighi *et al.*[15] examined CLI using their proposed efficient adaptive scheduling strategy for UL receptions from user 1 and DL transmissions to user 2, and demonstrated substantial performance improvements. Tian *et al.*[16] proposed a decentralized BS association approach tailored for adaptable duplex systems, aiming to optimize the overall network sum rate, where the BS association problem is formulated as a BS association game. Some research groups have also adjusted the UL/DL configuration to avoid CLI; this strategy can be applied to the cluster. Chen *et al.*[17] proposed a practical throughput model for the service, accounting for UL/DL bottlenecks in unmanned aerial vehicle (UAV)-assisted cellular network scenarios. They employed genetic schemes to devise a smart TDD UL/DL configuration algorithm. Esswie *et al.*[18] focused on the demand for ultrareliable and low-latency communications affected by CLI. In their research, emphasis is placed on proposing a semidynamic and computationally efficient TDD radio frame adaptation algorithm tailored for 5G macro deployments. Lee *et al.*[19] proposed an averaging algorithm aimed at mitigating CLI within a dynamic TDD system. This approach integrates both static and dynamic characteristics into a straightforward SINR-ordered arrangement. In addition, there are also some other coordination-based solutions to mitigate CLI. Liu *et al.*[20] proposed a hybrid TDD system to mitigate the interference and maintain the efficient operation of a flexible duplex. Esswis and Pedersen[21] proposed a TDD frame selection framework that is responsive to service requirements in multitraffic deployments. They assessed the performance of InF network deployments using contemporary 3GPP modeling assumptions. Lee *et al.*[22] proposed a decentralized approach for slot assignment to address CLI arising from dynamic TDD. The system requires the sharing of full or partial information on slot assignment and mutual interference among all cells to coordinate dynamic slot assignment.

Different from coordination-based solutions, a sensing-based scheme is also adopted to mitigate CLI. This is a complementary scheme that could be used prior to applying the following CLI mitigation solutions. The idea of the sensing-based scheme is to sense whether CLI occurs before transmission, thereby enabling the mitigation of CLI. The sensing-based scheme operates

in a distributed manner without the need for cooperation between adjacent cells and are attracting more attention both in academics and in the standardization of 5G. Tan *et al.*[23] focused on improving the accuracy of conventional channel modeling and proposed a polynomial CLI mitigation based on channel parameter estimation, along with two CLI cancellers leveraging machine learning (ML) techniques. Nwalozie *et al.*[24] combined the reconfigurable intelligent surface (RIS) with TDD and proposed two noniterative methods to maximize the spectral efficiency. Nwalozie and Haardt[25] also considered the RISs in the TDD system and proposed a joint optimization problem of transmit precoders of the BSs and the RIS reflection vector, which can improve the communication efficiency while reducing the impact of CLI. Compared with the academic sector, the industrial sector shows more interest in researching sensing-based schemes.[26,27] In Ref. 28, the listen-before-talk mechanism was introduced to protect the UL performance from interference originating from BS to BS transmissions.[28] Sensing should be performed by both the transmitter and the receiver to evade the hidden node issue proposed in Ref. 29, which can make it necessary to recalibrate the scheduling of the BS.[29] Different from this method, sensing performed by users has also been studied.[30] The BS can recalibrate the scheduling whether or not the user equipment (UE) undertakes channel sensing.

However, the existing work and standards may ignore or not mention the interference mitigation, feasibility analysis or gain verification of the CLI problem in an actual dynamical 5G-A heterogeneous-frame-structure network. In this paper, we address the pressing challenges faced by 5G-advanced networks in meeting the diverse demands of users and vertical industries, in the pursuit of flexibility in system design across both the physical and higher layers. Recognizing that a single-frame structure falls short in providing the required adaptability, we investigate a heterogeneous frame structure to accommodate various traffic modes. However, the proposed heterogeneous network also introduces a significant challenge in the form of the CLI problem, which adversely affects the network performance. To overcome this challenge, the practicality of the CLI mitigation method and the enhancement of the UL performance for the impacted micro-BS are validated using a physical verification platform. The main contributions are summarized below.

1) To meet the requirements for future networks, a heterogeneous-frame-structure (7D3U & 1D3U) 5G-A network is proposed to tackle the complex DL and UL demands arising from both public users and vertical industries.
2) To mitigate the CLI problem in a heterogeneous-frame-structure network, we propose methods 1 and 2 from the disturbed micro-BS side and method 3 or 4 from the scrambling macro-BS side depending on the macro-BS load.
3) We evaluate the performance of the proposed algorithms on the basis of experimental results. The combination of methods 1 and 2 is adopted by the micro-BS, and method 3 is adopted by the macro-BS when the load is low. As a result, complete CLI mitigation is achieved, and the disturbed micro-BS UL throughput is improved by 75.8%. The mitigation of CLI can be effectively achieved by using method 4, and the disturbed micro-BS UL throughput is improved by 57.4%.

The rest of the paper is structured as follows. Section 1 is an outline of the system architecture, and the formulated CLI problem is delineated. In Sect. 2, we delineate the four CLI

mitigation algorithms and their underlying principles. In Sect. 3, we present insights into the verification and analysis outcomes of the aforementioned methodologies. Finally, Sect. 4 is a summary of the paper.

2. Network Architecture Design

2.1 Link budget analysis

As seen in Fig. 2, the communication system consists of a macro-BS in the public network, the ToB network micro-BS, UE 1 attached to the macro-BS, and UE 2 attached to the micro-BS. The macro- and micro-BSs comprise the frame structure from slots 0 to 9, such as DDDSU DDSUU (DL, special, and UL slots), which is called 7D3U. Another DSUUU DSUUU mode is called 1D3U. The interference at the same frequency in the aforementioned heterogeneous-frame-based network can be divided into inter-BS and inter-UE interferences. The interference between BSs is the interference caused by the BS DL to the neighboring BS UL direction.

In slot 2, the downlink signal from the macro-BS will disrupt the UL reception of the micro-BS. Inter-UE interference arises from the adjacent UE UL that affects the DL of neighboring UEs. In slot 2, the UL transmission of UE2 will potentially interfere with the DL reception of UE 1. In this section, we concentrate on the modeling of interference between BSs and interference among UE, and analyze the central interference in this particular scenario by considering the link budget. Both types of interference are mainly composed of transceiver antenna gain, large-scale coupling loss, and small-scale coupling loss, as follows. Inter-BS interference can be described as

$$I_{BS} = \sum_{n} \frac{P_{BS}}{N} \cdot G_{T2} \cdot G_{R2} \cdot P_{L2} \cdot P_{S2}^{n,n}. \tag{1}$$

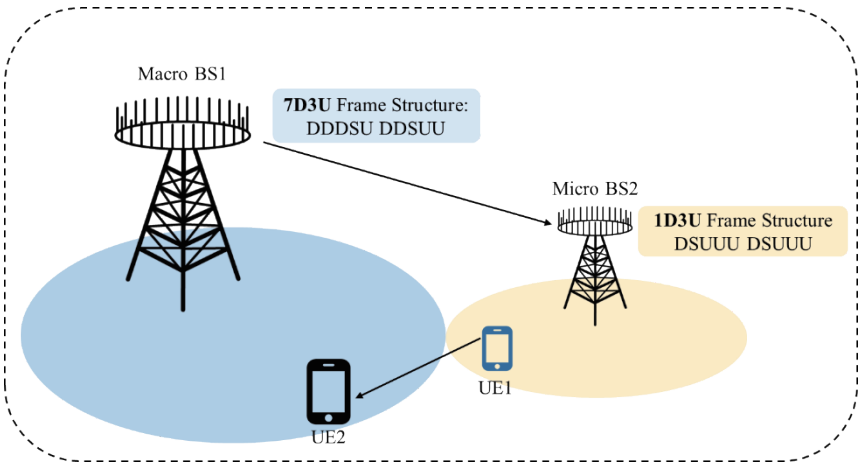

Fig. 2. (Color online) Overview of the macro–micro heterogeneous frame based network.

Inter-UE interference can be described as

$$I_{UE} = \sum_{n} \frac{P_{UE}}{M} \cdot G_{T1} \cdot G_{R1} \cdot P_{L1} \cdot P_{S1}^{n,n}. \tag{2}$$

The specific descriptions of the aforementioned parameters and variables are given in Table 1.

To assess the comparative magnitudes of inter-BS and inter-UE interferences in co-frequency and heterogeneous-frame-based networks, we refer to the path loss model in 3GPP Technical Report (TR) 38.901.[31] It uses the above interference model to analyze the link budget. For the urban macro (UMa) and indoor hot spot scenarios, the DL path loss from the macro-BS to the micro-BS and that from the macro-BS to the UE are as follows.

a) In the UMa line-of-sight (LOS) environment:

$$PL_{UMa\text{-}LOS} = \begin{cases} PL_1 & 10\ \text{m} \le d_{2D} \le d'_{BP} \\ PL_2 & d'_{BP} \le d_{2D} \le 5\ \text{km} \end{cases} \tag{3}$$

$$PL_1 = 28.0 + 22\log_{10}\left(d_{3\text{D}}\right) + 20\log_{10}\left(f_c\right) \tag{4}$$

$$PL_2 = 28.0 + 40\log_{10}\left(d_{3D}\right) + 20\log_{10}\left(f_c\right) - 9\log_{10}\left(\left(d'_{BP}\right)^2 + \left(h_{BS} - h_{UT}\right)^2\right) \tag{5}$$

Here, f_c is the working frequency, h_{BS} is the height of the base station, h_{UT} is the height of the UE, and d_{3D} is the distance between the BS and the UE.

b) In the UMa non-line-of-sight (NLOS) environment:

$$PL_{UMa\text{-}NLOS} = \max\left(PL_{UMa\text{-}LOS}, PL'_{UMa\text{-}NLOS}\right) \text{ for } 10\ \text{m} \le d_{2D} \le 5\ \text{km} \tag{6}$$

Table 1
System parameters.

Parameter	Description
P_{UE}	Maximum transmit power of UE
P_{BS}	Maximum transmit power of BS
$M1$	Number of UE uplink transmission bandwidth resource blocks (RBs)
N	Number of BS downlink bandwidth RBs
G_{T1}	Antenna gain of the scrambling UE transmitting antenna
G_{R1}	Antenna gain of the disturbed UE receiving antenna
G_{T2}	Antenna gain of the transmitting antenna of the scrambling BS
G_{R2}	Antenna gain of the disturbed BS receiving antenna
P_{L1}	Large-scale coupling loss between UEs
$P_{S1}^{n,n}$	Small-scale coupling loss of RB n of the disturbed UE to that of the disturbed UE
P_{L2}	Large-scale coupling loss between macro- and micro-BSs
$P_{S2}^{n,n}$	Small-scale coupling loss of RB n of the macro-BS to that of the micro-BS
n	RB index; the same RB index represents the same frequency domain location

$$PL'_{UMa-NLOS} = 13.54 + 39.08\log_{10}\left(d_{3D}\right) + 20\log_{10}\left(f_c\right) - 0.6\left(h_{UT} - 1.5\right) \tag{7}$$

For the indoor hot spot and urban macro (UMi) situation, under indoor-home model InH-Office, the UL path loss equation from the UE to the micro-BS is as follows.

a) In the LOS environment:

$$PL_{InH\text{-}LOS} = 32.4 + 17.3\log_{10}\left(d_{3D}\right) + 20\log_{10}\left(f_c\right) \tag{8}$$

b) In the UMa NLOS environment:

$$PL_{InH\text{-}NLOS} = \max\left(PL_{InH\text{-}LOS}, PL'_{InH\text{-}NLOS}\right) \tag{9}$$

$$PL'_{InH\text{-}NLOS} = 38.3\log_{10}\left(d_{3D}\right) + 17.30 + 24.9\log_{10}\left(f_c\right) \tag{10}$$

For the UMa scene, under the UMi Street Canyon model, the path loss equation from one UE to another UE is as follows.

a) In the LOS environment:

$$PL_{UMi\text{-}LOS} = \begin{cases} PL_1 & 10\text{ m} \le d_{2D} \le d'_{BP} \\ PL_2 & d'_{BP} \le d_{2D} \le 5\text{ km} \end{cases} \tag{11}$$

$$PL_1 = 32.4 + 21\log_{10}\left(d_{3D}\right) + 20\log_{10}\left(f_c\right) \tag{12}$$

$$PL_2 = 32.4 + 40\log_{10}\left(d_{3D}\right) + 20\log_{10}\left(f_c\right) - 9.5\log_{10}\left(\left(d'_{BP}\right)^2 + \left(h_{BS} - h_{UT}\right)^2\right) \tag{13}$$

Here, d_{2D} is the coverage radius of the BS.

b) In the NLOS environment:

$$PL_{UMi\text{-}NLOS} = \max\left(PL_{UMi\text{-}LOS}, PL'_{UMi\text{-}NLOS}\right) \text{ for } 10\text{ m} \le d_{2D} \le 5\text{ km} \tag{14}$$

$$PL'_{UMi-NLOS} = 35.3\log_{10}\left(d_{3D}\right) + 22.4 + 21.3\log_{10}\left(f_c\right) - 0.3\left(h_{UT} - 1.5\right) \tag{15}$$

According to interference [Eq. (1)] between BSs, it is assumed that the macro-BS spacing is 500 m and the transmission power is 53 dBm (200 W), while the spacing between the macro-BS and the micro-BS is 150 m. The UE's UL transmission power to the micro-BS is 23 dBm, and the micro-BS is situated 50 m away from the UE. It can be deduced that the LOS path loss between the macro-BS and the micro-BS is 86.76 dB, the NLOS path loss is 104.36 dB, and the

NLOS path loss of the UE to the micro-BS is 95.92 dB. The link budget analysis in Table 2 shows that the NLOS interference signal received for the transmission from the micro-BS to the macro-BS is 9.56 dB larger than the UL signal received for the transmission from the micro-BS to the UE. If the inter-BS CLI is not eliminated or mitigated, the UL of the micro-BS will be subject to severe interference.

According to interference [Eq. (2)] between UEs, it is assumed that the macro-BS spacing is 500 m, the transmission power is 53 dBm, and the spacing between the macro-BS and UE1 is 150 m. The UL transmission power of the UE is 23 dBm, and the distance between UE2 and UE1 is 30 m. Under the above assumptions, combined with the path loss model in the 3GPP TR 38.901 protocol, it can be deduced that the path loss between the macro-BS and UE1 is 104.36 dB, and the path loss between UE2 and UE1 is 86.13 dB. As seen from the link budget analysis results in Table 3, the interference signal strength experienced by UE1 to UE2 is analogous to the DL signal received by the macro-BS.

Because of the UE's low transmission power and the fact that the inter-UE channel is generally dominated by NLOS, the inter-UE interference is fairly controllable. However, the BS transmission power is enormous, and LOS rapidly occurs between BSs, especially in the scenario where the BS is deployed at a higher location. Thus, addressing inter-BS interference emerges as a pressing challenge in the context of heterogeneous-frame-based networks. Next, we will focus on the analysis of inter-BS interference in heterogeneous-frame-based network scenarios.

Table 2
Results of inter-BS interference link budget analysis of heterogeneous-frame-based network.

Parameter	Macro-BS → Micro-BS	UE → Micro-BS
Transmission power	53 dBm	23 dBm
Transmit antenna gain	8 dBi	0 dBi
Path loss	LOS: 86.76 dB (150 m)	NLOS: 95.92 dB (50 m)
Penetration loss	20 dB	0 dB
Receiving antenna gain	8 dBi	8 dBi
Receiving power	LOS: −37.76 dBm	NLOS: −64.92 dBm

Table 3
Results of inter-BS interference link budget analysis of heterogeneous-frame-based network.

Parameter	Macro-BS → Micro-BS	UE → Micro-BS
Transmission power	53 dBm	23 dBm
Transmit antenna gain	8 dBi	0 dBi
Path loss	LOS: 86.76 dB (150 m) NLOS: 104.36 dB(150 m)	NLOS: 95.92 dB (50 m)
Penetration loss	20 dB	0 dB
Receiving antenna gain	8 dBi	8 dBi
Receiving power	LOS: −37.76 dBm NLOS: −55.36 dBm	NLOS: −64.92 dBm

2.2 5G-RAN intelligent architecture

The intelligent architecture of the 5G radio access network (5G-RAN) can be categorized into the following three layers, proceeding from the bottom to the top: infrastructure layer, self-intelligent application layer, and business operation layer. The business operation layer mainly carries out cross-domain intelligent business activities, including closed-loop operation and maintenance, computing power coordination, and business orchestration. The RAN composer wireless single-domain intelligent scheme is considered in the self-intelligence application and infrastructure layers. Guided by the latest intention-driven technology in the industry, the scheme focuses on multivalue scenarios and provides operators with self-intelligent applications in different scenarios. At the same time, the scheme supports capacity opening and cross-domain closed-loop upwards and twin evolution and single-domain closed-loop downwards with the computing power, data, and algorithms of the infrastructure layer. The heterogeneous frame structure interference mitigation scheme is based on the application of a typical platform architecture, as shown in Fig. 3, which can improve the ability and application effect of interference resolution.

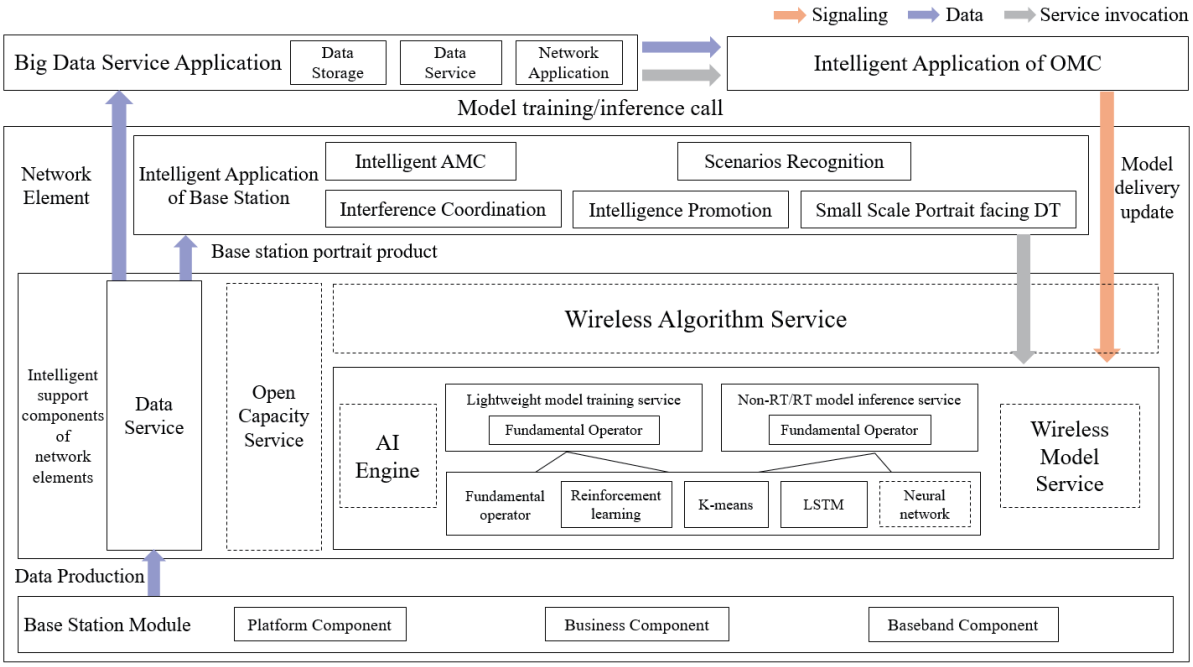

Fig. 3. (Color online) Design of 5G-RAN system architecture.

3. Algorithm Design

3.1 Algorithm design

When the micro-BS's frame structure is adaptively adjusted to the 1D3U configuration, the macro- and micro-BSs form a heterogeneous network, and the following four CLI mitigation methods will be introduced: slot-level AMC adaptive scheduling, interference mitigation algorithm, adaptive slot turn-off, and edge user adaptive scheduling. These four algorithms can be used separately or iteratively.

3.2 Adaptive frame structure adjustment

When the UL service demand of micro-BS2 is high, the frame structure can be adjusted to the UL-based frame-structure configuration adaptively, such as 1D3U (DSUUU DSUUU), as shown in Fig. 4. In various application scenarios, different methods can be employed to determine business requirements and the frame structure is adapted accordingly. For instance, in a typical business scenario, historical traffic data analysis can be employed to predict future traffic requirements. When the demand exceeds a predefined threshold, slot resources can be adjusted accordingly.

Firstly, the initial frame structure of the macro- and micro-BSs is configured to be 7D3U. The macro- and micro-BSs have the same frequency and frame network, and there is no CLI. Secondly, on the basis of network load, if the UL Physical Resource Block (PRB) utilization rate of the micro-BS is greater than the large UL activation threshold and such a status holds true for more than X seconds, the micro-BS slot configuration can be adapted in the range from 7D3U to 1D3U. Lastly, on the basis of the results of network load monitoring, if the UL PRB resource utilization of the micro-BS is less than the large UL activation threshold and is maintained for more than X seconds, the micro-BS slot configuration remains unchanged at 7D3U or is adaptively adjusted back to 7D3U from 1D3U. Macro- and micro-BSs currently restore the same

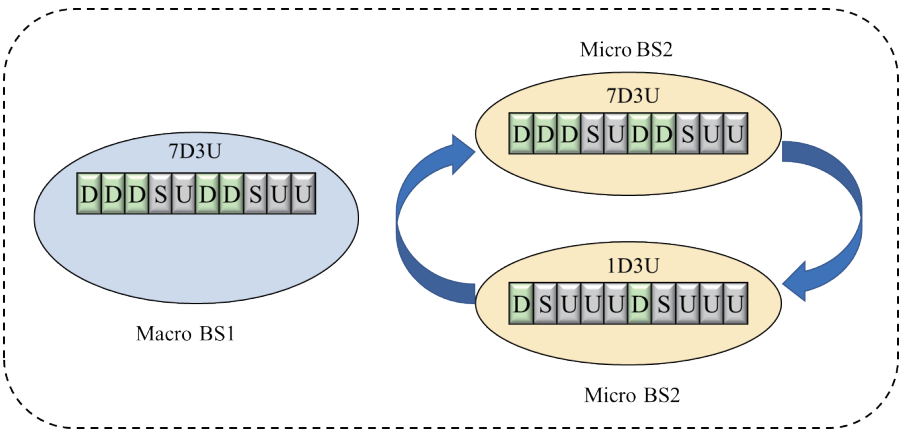

Fig. 4. (Color online) Macro-BS (7D3U) and micro-BS (1D3U) heterogeneous-frame-structure networks.

frequency, and there is no CLI. This method can be set by a large UL activation threshold and the value of the maintenance time X in accordance with the actual needs. On the basis of the results of the precise measurement of the current network, the typical value of the large UL threshold can be set to (60–90%) + hys (Hysteresis), where hys can be set to about 3% to prevent jitter. The typical value of X can be set to 10 s.

3.3 Slot-level AMC scheduling

In the general UL AMC inner-loop adaptive scheduling method,[32] all slots in the time domain are measured and encoded. The general UL AMC averages the channel quality over all slots, which can lead to an overestimation of the quality of the slot channel that is subjected to heavy interference from the macro-BS. In the heterogeneous frame structure networks, such as the macro-BS with 7D3U and the micro-BS with 1D3U, only slot 2 has all-symbol CLI. For slots 3 and 7, only a part of symbols in the slot suffers CLI, while for other UL slots (i.e., slots 4, 8, and 9), there is no CLI. After all the slots are averaged, the overall channel quality is underestimated for at least slots 4, 8, and 9, the coding efficiency is not high, and the UL rate is low. For slot 2, a coding efficiency clearly higher than the actual requirement will be used, which may cause the UL transmission to not be received correctly and affect the UL throughput of the system.[33]

To address the above issues, an adaptive scheduling method for slot-level inner loop AMC is introduced. The micro-BS on the disturbed side adaptively adjusts the coding level of modulation on the basis of the degree of interference and channel quality, automatically performs dynamic link adaptive scheduling in accordance with the position and intensity of the disturbed slot, and automatically reduces the bit rate of the disturbed slot. The slot-level inner loop AMC adaptive scheduling configures multiple sets of AMC resources for each UE to make the measured channel quality more accurate. Three sets of AMC resources are configured for each UE, and different slot locations are mapped to different AMC categories. For example, slot 2 is mapped to AMC-1, slots 3 and 7 are mapped to AMC-2, and slots 4, 8, and 9 are mapped to AMC-3, as seen in Table 4.

Table 4
AMC adaptive scheduling methods.

UL direction	General AMC adaptive scheduling method	Slot-level inner loop AMC adaptive scheduling method		
AMC mode	AMC	AMC-1	AMC-2	AMC-3
Slot location	2, 3, 4, 7, 8, 9	2	3, 7	4, 8, 9
SINR estimate	The overall channel quality is underestimated and the rate is low.	All-symbol interference	Partial symbol interference	No interference

3.4 Interference mitigation algorithm

3.4.1 Super-MIMO technology

To enhance the UL-interference mitigation capability of a disturbed BS, one approach is to expand the size of the receiving antenna. For instance, the Super-MIMO technology can be employed to increase the cell's receiving antenna array size by using distributed small antennas to form a super large antenna array.[34] Theoretically, this expansion can improve the UL interference mitigation capability by 9 dB.

As shown in Fig. 5, multiple indoor four transmission and reception (4TR) distributed small antennas form a large antenna array; for example, 8 × 4TR antennas form a 32TR Super-MIMO cell. Distributed antennas are calibrated for phase alignment by exchanging calibration signals through an air interface. In this way, not only the downstream power superposition benefit but also the joint beam-forming benefit can be obtained. In terms of the benefits of UL reception, not only can large-scale antenna arrays be used for joint channel estimation for multi-user MIMO, but also interference mitigation can be improved through joint equalization.

3.4.2 Interference rejection combining technology

The fundamental concept of interference rejection combining (IRC) equalization in wireless communication primarily involves the equalization of channel characteristics. In this context, the equalizer at the receiving end produces characteristics that are inversely related to those of the channel, aiming to mitigate the intersymbol interference induced by the time-varying multipath propagation characteristics of the channel. The IRC technology is often used for equalization, which can be considered as an advanced diversity reception function that can improve the quality of the UL and increase the gain of the UL signal. In Fig. 6, *s* is the actual signal transmitted by the transmitter; it passes through the air interface of channel h and is superimposed with noise n. Finally, r is the actual air-interface received signal, and the receiver

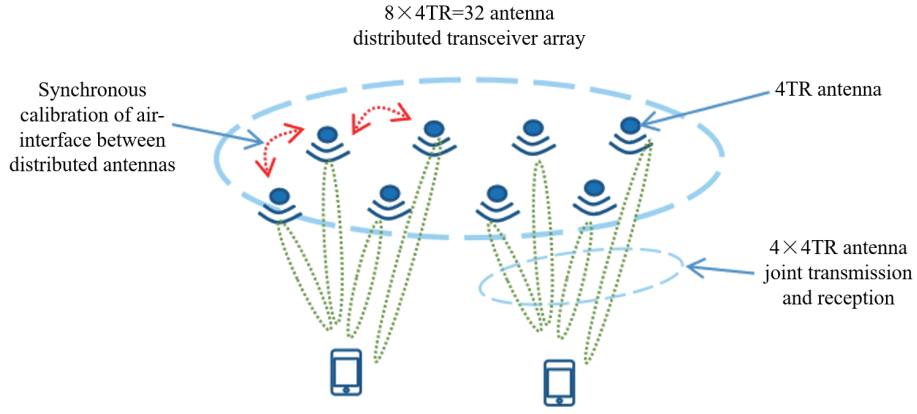

Fig. 5. (Color online) 8 × 4TR antennas form a 32TR super-MIMO cell for interference mitigation.

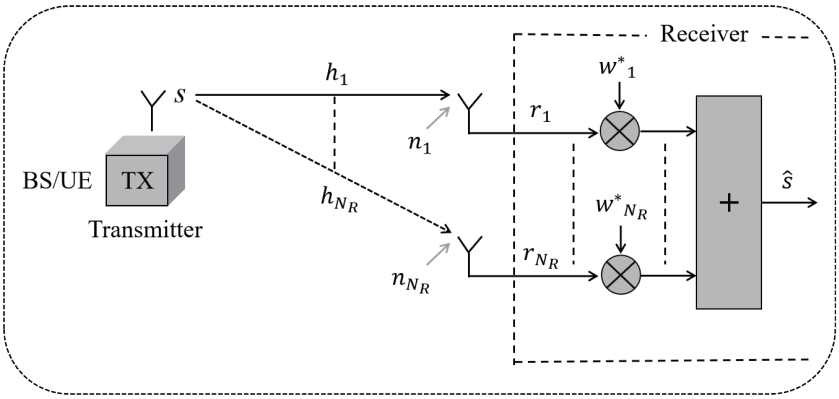

Fig. 6. Architecture of IRC equalization frame.

is expected to recover signal s at the receiving end through IRC equalization.

Assuming that the sent signal s passes through a non-frequency-selective fading channel (that is, time dispersion without a wireless channel) and white noise, the received signal can be represented as

$$\overline{r} = \begin{pmatrix} r_1 \\ \vdots \\ r_{N_R} \end{pmatrix} = \begin{pmatrix} h_1 \\ \vdots \\ h_{N_R} \end{pmatrix} \cdot s + \begin{pmatrix} n_1 \\ \vdots \\ n_{N_R} \end{pmatrix} = \overline{h} \cdot s + \overline{n}. \tag{16}$$

The recovery of the sent signal s can be expressed in vector terms as

$$\hat{s} = [w_1^* \cdots w_{N_R}^*] \cdot \begin{bmatrix} r_1 \\ \vdots \\ r_{N_R} \end{bmatrix} = \overline{w}^H \cdot \overline{r}. \tag{17}$$

The measurement of w in IRC then becomes critical. To maximize the signal-to-noise ratio after the linear combination of signals, the weight vector $\overline{w}$ must satisfy the following relationship:

$$\overline{w}_{MRC} = \overline{h}. \tag{18}$$

In Super-MIMO, the original four-antenna receiver has been enhanced to a 32-antenna receiver, which can make the measurement of w more accurate and achieve higher interference cancellation effects. The entire IRC calculation model assumes that the signal sent by the sender is X, the signal received by the receiver is Y, and N is the interference noise. The transmission model can be described as

$$Y = HX + N. \tag{19}$$

The estimated model can be described as

$$\hat{X} = W^H Y. \tag{20}$$

The equation of estimation error e is

$$e = \hat{X} - X. \tag{21}$$

The cost function mean squared error is defined as $E\|e\|^2$, and it must satisfy the weight of $\arg\min_w E\|e\|^2$, i.e.,

$$\begin{aligned} \|e\|^2 &= tr\left\{\left(W^H Y - X\right)\left(W^H Y - X\right)^H\right\} \\ &= tr\left\{W^H HXX^H H^H W + W^H HXN^H W - W^H HXX^H + W^H NX^H H^H W \right. \\ &\quad \left. + W^H NN^H W - W^H NX^H - XX^H H^H W - XN^H W + XX^H\right\}. \end{aligned} \tag{22}$$

According to the relationship $E(XN^H) = 0$, $E(NN^H) = R_{nn}$, $E(XX^H) = R_{xx}$,

$$\begin{aligned} E\|e\|^2 = tr\left\{W^H HXX^H H^H W - W^H HXX^H + W^H NN^H W - XX^H N^H W \right. \\ \left. - XX^H H^H W + XX^H\right\}. \end{aligned} \tag{23}$$

When the derivative equation satisfies the condition $dE\|e\|^2/dW^H = 0$, the extreme values $dE\|e\|^2/dW^H = 0$ can be determined as

$$\frac{dE\|e\|^2}{dW^H} = \frac{dtr\left\{W^H HR_{xx}H^H W - W^H HR_{nn} + W^H R_{nn}W - R_{xx}H^H W + R_{xx}\right\}}{dW^H}. \tag{24}$$

From the equation above, we can obtain

$$HR_{nn}H^H W - HR_{xx} + R_{nn}W = 0. \tag{25}$$

Hence, the final weight W can be obtained as

$$W = (HR_{xx}H^H + R_{nn})^{-1} HR_{xx}. \tag{26}$$

3.5 Adaptive slot turn-off

Building on the heterogeneous network, if the macro-BS monitors the frame structure change of the micro-BS to 1D3U or receives vital CLI feedback from the micro-BS and detects that the

macro-BS DL PRB utilization rate is less than the slot turn-off threshold 1 and is maintained for more than X seconds according to network load monitoring, then the macro-BS can perform slot turn-off at a specific slot location, such as DL slots 2, 3, and 7. If the DL PRB utilization of the macro-BS is greater than the slot turn-off threshold 2 and is maintained for more than X seconds, the macro-BS cancels the slot turn-off. According to the actual measurement results of the current network, the slot turn-off threshold 1 can be appropriately configured with a typical value of (50–60%) −hys, and the slot turn-off threshold 2 can be appropriately configured with a typical value of (80–90%) + hys. Among them, hys can be set to about 3% to prevent jitter and X can be set to 10 s. The slot turn-off approach is suitable for scenarios where the network load of the disturbance BS is not high, as shown in Fig. 7.

3.6 Edge user adaptive scheduling

The DL signal from the BS can be directional through the utilization of digital precoding or analog beamforming.[35] The traditional adaptive coordinated beamforming scheme needs real-time signaling interaction on the spatial domain information, which requires an ideal backhaul link between BSs. The core idea of the edge user adaptive scheduling method is to identify potential edge users and then the BS inhibits scheduling these users in slots that may cause CLI, thereby reducing the interference. This method has minimal impact on the scheduling and performance of the macro-BS, but it can reduce the interference between BSs. In addition, after triggering the edge user adaptive scheduling method, the BS only needs to identify edge UEs and schedule them on specified resources, through which the overhead and real-time requirements for signaling interaction are reduced.

As shown in Fig. 8, UE1 and UE2 are attached in the macro-BS. UE1 is positioned in the cell's central area. On the macro-BS1 side, beam 1 transmits DL signals to UE1. Since the beam direction is far from the direction toward micro-BS2, the interference between BSs is negligible. UE2 is situated either at the cell periphery or within the overlapping region served by both the macro- and micro-BSs. Macro-BS1 transmits the DL signal to UE2 through beam 2. Because the beam direction is close to the direction toward micro-BS2, the interference between BSs is extensive. Therefore, this scenario can adopt an edge user adaptive scheduling method, which is described below.

1) In the macro–micro frame networking environment, the micro-BS detects its UL interference in real time, including interference intensity, time domain position, and interference type.

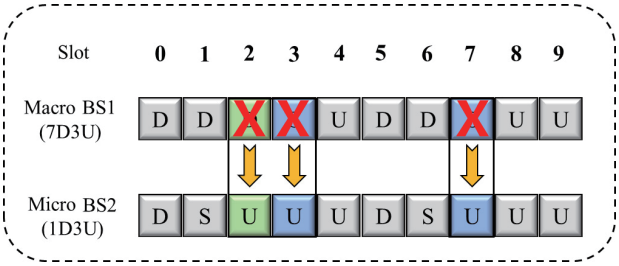

Fig. 7. (Color online) Macro-BS adaptive turn-off of slots 2, 3, and 7 to mitigate CLI towards the micro-BS.

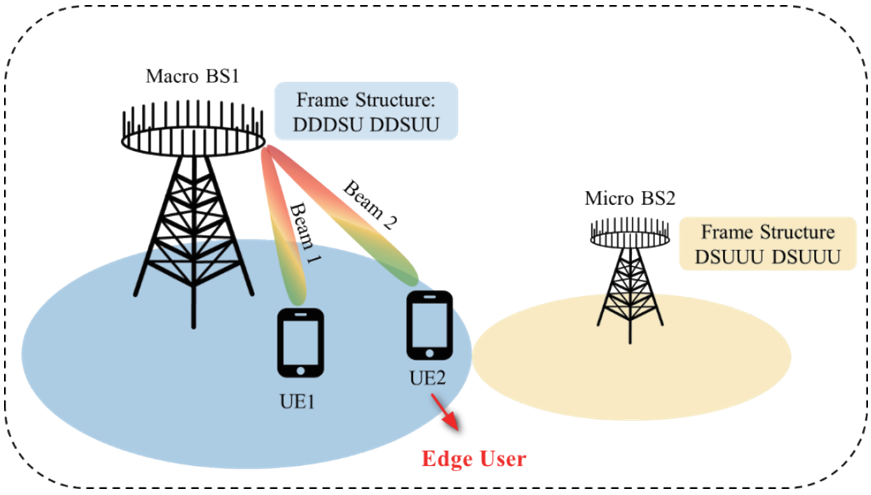

Fig. 8. (Color online) Edge users are restricted from using slots 2, 3, and 7 of macro-BS.

2) If interference is determined to be CLI, the interference mitigation request to the macro-BS is triggered (the interference coordination request can be sent to the macro-BS through the X_n interface between BSs), and the macro-BS is expected to perform edge user adaptive scheduling.
3) After the macro-BS receives the interference coordination request, the macro-BS's own DL PRB utilization information is determined. If the DL PRB utilization is less than the slot turn-off threshold 1 and is maintained for more than X seconds, the macro-BS adopts the adaptive slot turn-off method. For example, in this case, slots 2, 3, and 7 are turned off . If the macro-BS DL PRB utilization is more than the slot turn-off threshold 2 and is maintained for more than X seconds, the macro-BS cancels the adaptive slot turn-off in method 2 and performs the edge user adaptive scheduling.
4) The macro-BS sends an A3 event same-frequency neighbor measurement control message to the UE to trigger the UE measurement report (MR) after the A3 event. If the neighborhood information in the MR contains a micro-BS, that is, the UE is in the overlapping area of the macro- and micro-BSs, it is established that the UE is positioned at the periphery of the macro-BS.
5) The macro-BS limits the DL traffic scheduling of UE2 in slots 2, 3, and 7, but UE2 can be scheduled in other slots, such as slots 0, 1, 5, and 6. The macro-BS does not limit the DL service of UE1 with large airspace isolation and can use all DL slots.

4. Experimental Tests and Analysis

4.1 Scenario and configuration setting

As seen in Fig. 9, to validate the viability of the CLI mitigation approach and assess its impact on enhancing the UL performance gains for the micro-BS, micro-BSs are placed in a

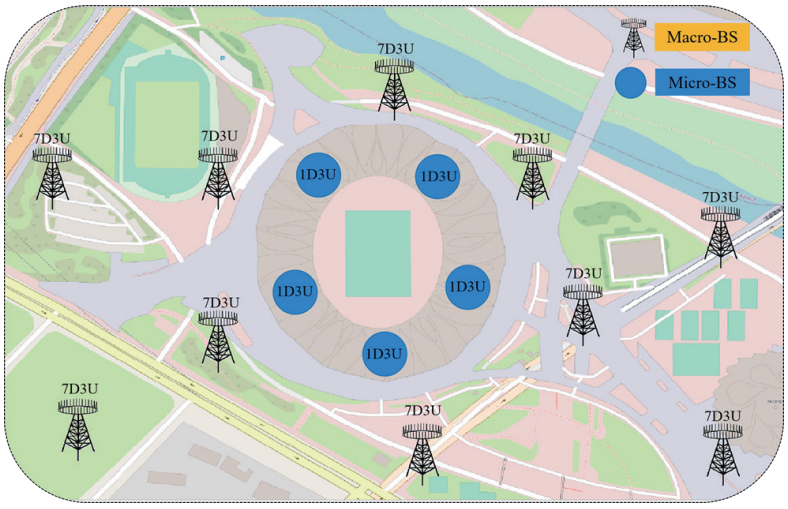

Fig. 9. (Color online) Verification scenario selection.

gymnasium, and there are macro-BSs arranged about 100 m outside the gymnasium. Macro- and micro-BSs adopt the default 7D3U slot configuration. The macro-BSs adopt the current network 64TR active antenna unit (AAU) equipment, and the software version is the current network commercial version. The indoor micro-BSs adopt a digital room pico remote radio unit (pRRU). The macro-BSs are mainly used for networks serving private users. The micro-BSs in the gymnasium are mainly used for meeting UL communication requirements such as those for high-definition video backhaul or live broadcast. The micro-BS in the gymnasium is interfered by CLI between the BSs and the outdoor macro-BS. To validate the practicality and performance improvement of the CLI mitigation approach, the specific control groups and technical strategies for comparative analysis were selected.

4.2 Results and analysis

Table 5 shows the performance improvement of each solution (multi-CLI mitigation method) on macro- and micro-BSs. The default isomorphic configuration of micro-BSs resulted in a UL throughput of 268.3 Mbps with the UL modulation and coding scheme (MCS) of 21.7 (default baseline; macro- and micro-BSs are configured with 7D3U), after adaptive frame structure adjustment in micro-BSs in the 7D3U-to-1D3U configuration, which is composed of macro- and micro-BS heterogeneous networks. The UL MCS of micro-BSs decreased from 21.7 to 9.2, whereby the UL throughput decreased to 168.8 Mbps. As can be observed from the change of the UL MCS of micro-BSs, although more UL resources can be obtained, this is still insufficient to compensate for the performance degradation caused by significant CLI that remains unaddressed following the adaptive frame structure adjustment, further requiring mitigation strategies.

Then, with the combined method 1&2 (Solution 1) implemented in the micro-BSs, the UL MCS increased from 9.2 to 17.5, which improved the UL throughput to 332.8 Mbps. The CLI still exists as the UL MCS is still lower than that of the baseline case. However, it has been

Table 5
Micro-BS KPI results obtained using different solutions.

Contrast	Micro-BS	Macro-BS	RSRP (dBm)	DL MCS	UL MCS	UL throughput (Mbps)
Default baseline	7D3U	7D3U	−78.7	22.3	21.7	268.3
Heterogeneous network	1D3U	7D3U	−78.4	22.8	9.2	168.8
Solution 1	Method 1&2	7D3U	−78.1	22.5	17.5	332.8
Solution 2-1	Method 1&2	Method 3	−78.9	23.4	25.3	471.7
Solution 2-2	Method 1&2	Method 4	−78.6	23.1	23.8	422.3

considerably reduced compared with no CLI mitigation, and the UL throughput has been increased to some extent owing to more UL resources. When method 1&2 is implemented in micro-BSs, method 3 is deployed in the macro-BS if its load is low (Solution 2-1), which increases the UL MCS from 9.2 to 25.3 and the micro-BSs UL throughput from 168.8 to 471.7 Mbps. By turning off part of DL slots of the macro-BS, CLI and legacy interference such as UE-to-BS interference are effectively inhibited in these slots. A higher UL MCS than the baseline case is obtained, and the UL throughput is significantly increased. On other hand, when the macro-BS DL load is high, method 4 is deployed (Solution 2-2). Under this condition, the UL MCS improved from 9.2 to 23.8 and the micro-BS UL throughput increased to 422.3 Mbps. Clearly, the DL slot turn-off is unreasonable in the case of high macro-BS DL load. Edge user adaptive scheduling can considerably reduce CLI to a similar level as the legacy interference under the baseline case without affecting the DL throughput.

As seen in Fig. 10, compared with the default baseline, the micro-BS UL throughput deteriorated by 37.1% because of CLI in the heterogeneous network. With the deployment of solution 1 on micro-BSs, the micro-BS UL throughput improved by 24.0%, whereas solution 2-1 and solution 2-2 achieved improvements of 75.8 and 57.4%, respectively. Other relative key point indicators (KPIs), such as average RSRP and DL MCS, remain stable or only slightly fluctuate. It is clear that the implementation of the above solutions only improves the UL direction of the micro-BS and has no impact on the DL direction of the micro-BS. Both the DL and UL throughputs of the macro-BS remain stable with the implementation of the above solutions.

The proposed methods have lower implementation complexity, more application scenarios, and more significant performance improvements than traditional CLI mitigation schemes. Firstly, considering the delay and overhead of inter-BS interaction, information cannot be frequently exchanged between different BSs in real time. As a result, the solution that requires a real-time information interaction is not feasible in actual deployment. In addition, some information is not suitable for interaction between BSs from the perspective of security. However, most of the information that needs to be exchanged between BSs in traditional CLI mitigation schemes requires real-time interaction. For example, the scheduling information, interference level information, and Tx/Rx beam index should be exchanged in the scheduling and spatial domain coordination schemes.[12] However, for the proposed methods, only some semi-static information is required to be exchanged between the micro-BSs and the macro-BS. This includes the semi-static frame structure configuration used for AMC grouping within the slot-level AMC scheduling method, as well as the CLI measurement result needed to trigger

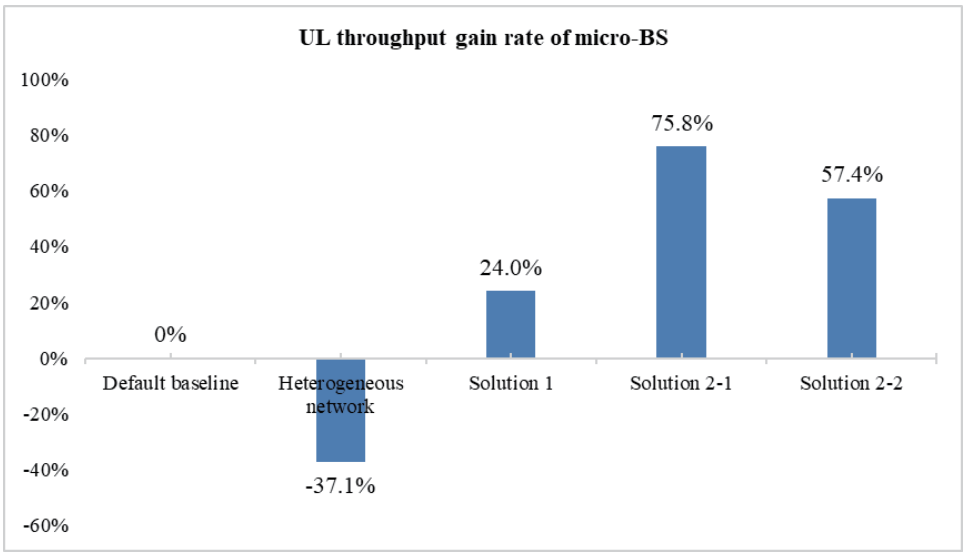

Fig. 10. (Color online) UL throughput gain rate of micro-BS.

adaptive slot turn-off or edge user adaptive scheduling. Secondly, the proposed methods can be applicable to different application scenarios with considerable performance gains. Compared with the traditional mechanism, it has clear advantages. For example, Razlighi *et al.*[15] proposed an optimal distributed dynamic time-division-duplex (D-TDD) scheme for the adaptive scheduling of its uplink receptions and downlink transmissions by taking into account intercell interference. Compared with the semi-static TDD, a maximum of 41% uplink rate gain can be obtained by the proposed scheme.[15] Under the same conditions, it is expected that there will be a significant gap from the available gains (75.8 and 57.4% for macro-BSs with low and high loads, respectively) of the methods proposed here.

Through the verification of multi-CLI mitigation methods, multiple sets of solution combinations under different network load scenarios of macro- and micro-BSs that can accurately meet the needs of different industries and realize diversified values of different scenarios under a single 5G-A network are identified.

5. Conclusions

In this study, a heterogeneous frame structure was proposed, and link budget and feasibility verification were performed to assess CLI generated under the scheme. Inter-BS interference was identified as the main interference in heterogeneous frame structures. On this basis, the following four methods were proposed: slot-level inner loop AMC adaptive scheduling, interference mitigation algorithm, adaptive slot turn-off, and edge user adaptive scheduling. Four sets of comparison experiments were designed for the separate use or combination scenario. The experimental results showed that when macro- and micro-BSs default to the 7D3U configuration, the UL throughput of the micro-BS can reach 268.3 Mbps, which is close to the

theoretical peak value. When the disturbed micro-BS adopted solution 1, the UL throughput increased to 332.8 Mbps (improvement of 24.0%). The UL throughput increased to 471.7 Mbps (improvement of 75.8%) under the macro-BS low load scenario and to 422.3 Mbps (improvement of 57.4%) when the macro-BS load was high.

References

1 D. Wang, W. Wang, H. Gao, Z. Zhang, and Z. Han: IEEE Trans. Wireless Commun. Methods Phys. Res., Sect. A **1** (2023) 1. https://doi.org/10.1109/TWC.2023.3291198
2 Y. Mao, C. You, J. Zhang, K. Huang, and K. B. Letaief: IEEE Commun. Surv. Tutorials. Methods Phys. Res., Sect. A **19** (2017) 2322. https://doi.org/10.1109/TWC.2023.3291198
3 M. Z. Chowdhury, M. Shahjalal, S. Ahmed, and Y. M. Jang: IEEE Open J. Commun. Soc. Methods Phys. Res., Sect. A **1** (2020) 957. https://doi.org/10.1109/OJCOMS.2020.3010270
4 L. Azpilicueta, P. Lopez-Iturri, J. Zuñiga-Mejia, M. Celaya-Echarri, F. A. Rodríguez-Corbo, C. Vargas-Rosales, and F. Falcone: Sensors. Methods Phys. Res., Sect. A **20** (2020) 5360. https://doi.org/10.3390/s20185360
5 W. Jiang, B. Han, M. A. Habibi, and H. D. Schotten: IEEE Open J. Commun. Soc. Methods Phys. Res., Sect. A **2** (2021) 334. https://doi.org/10.1109/OJCOMS.2021.3057679
6 B. Yu, L. Yang, H. Ishii, and S. Mukherjee: IEEE J. Sel. Areas Commun. Methods Phys. Res., Sect. A **33** (2015) 1201. https://doi.org/10.1109/JSAC.2015.2417013
7 F. Pan, X. Zhao, B. Zhang, P. Xiang, M. Hu, and X. Gao: Sensors. Methods Phys. Res., Sect. A **23** (2023) 8139. https://doi.org/10.3390/s23198139
8 3GPP. Technical specification group radio access network: (2017). http://www.3gpp.org/DynaReport/36913.htm
9 3GPP. Technical Specification Group Radio Access Network; NR (2019). http://www.3gpp.org/DynaReport/38901.htm
10 J. Kerttula, A. Marttinen, K. Ruttik, R. Jäntti, and M. N. Alam: EURASIP J. Wireless Commun. Networking. Methods Phys. Res., Sect. A **2016** (2016) 1. https://doi.org/10.1186/s13638-016-0696-z
11 H. Kim, J. Kim, and D. Hong: IEEE Commun. Surv. Tutorials. Methods Phys. Res., Sect. A **22** (2020) 2315. https://doi.org/10.1109/COMST.2020.3008765
12 A. Lukowa and V. Venkatasubramanian: Personal, Indoor and Mobile Radio Communications (IEEE, 2018). https://doi.org/10.1109/pimrc.2018.8580681
13 Q. Xin, H. Gao, and T. Lv: 2018 IEEE Int. Conf. Communications Workshops (ICC Workshops) (IEEE, 2018). https://doi.org/10.1109/ICCW.2018.8403526
14 Z. Yu, K. Wang, H. Ji, X. Li, and H. Zhang: China Commun. Methods Phys. Res., Sect. A **13** (2016) 1. https://doi.org/10.1109/CC.2016.7513198
15 M. M. Razlighi, N. Zlatanov, and P. Popovski: On Distributed Dynamic-TDD Schemes for Base Stations with Decoupled Uplink-Downlink Transmissions[C]//2018:1-6. https://doi.org/10.1109/ICCW.2018.8403595
16 S. Tian, M. Ma, and B. Jiao: Global Communications Conf. (IEEE, 2017). https://doi.org/10.1109/glocomw.2017.8269188
17 J. Chen, Y. Meng, W. Wang, X. Liu, and F. Liu: 2023 IEEE/CIC Int. Conf. Communications in China (IEEE, 2023) 1–6.
18 A. A. Esswie, K. I. Pedersen, and P. E. Mogensen: 2020 IEEE Wireless Communications and Networking Conf. (IEEE,2020) 1–6.
19 J. W. Lee, C. G. Kang, and M. J. Rim: 2018 Int. Conf. Information Networking (IEEE, 2018) 359–361.
20 C. T. Liu, J. Y. Pan, C. K. Huang, and W. Pao: 2020 Asia-Pacific Signal and Information Processing Association Annual Summit and Conf. (IEEE, 2020) 1588–1593.
21 A. A. Esswie and K. I. Pedersen; Analysis of Outage Latency and Throughput Performance in Industrial Factory 5G TDD Deployments.2020[2024-02-07]. https://doi.org/10.48550/arXiv.2012.05507
22 J. Lee, M. Rim, and C. G. Kang: IEEE Access. Methods Phys. Res., Sect. A **9** (2021) 63567. https://doi.org/10.1109/ACCESS.2021.3074176
23 J. S. Tan, S. Yang, K. Meng, J. Zhang, Y. Tang, Y. Bu, and G. Wang: IEEE Wireless Commun. Lett. Methods Phys. Res., Sect. A **7** (2023) 1269. https://doi.org/10.1109/LWC.2023.3270423

24 G. C. Nwalozie, K. Ardah, and M. Haardt: 2022 IEEE 12th Sensor Array and Multichannel Signal Processing Workshop. (IEEE, 2022) 36–40.
25 G. C. Nwalozie and M. Haardt: 2023 31st European Signal Processing Conf. (EUSIPCO). (IEEE, 2023) 1688-1692. https://doi.org/10.23919/EUSIPCO58844.2023.10289836
26 3GPP. On Cross-Link Interference Mitigation for Duplexing Flexibility, Tsg ran wg1 meeting, 2017. R1-1701669.
27 3GPP. Discussions on Cross-Link Interference Mitigation Schemes, Tsg ran wg1 meeting, 2017. R1-1701929.
28 3GPP. Dynamic TDD Performance Evaluation, Tsg ran wg1 meeting, 2017. R1-1704056.
29 3GPP. Channel Sensing Based Scheme for Cross-Link Interference Mitigation in NR, Tsg ran wg1 meeting, 2017. R1-1701617.
30 3GPP. Interference Management in NR, Tsg ran wg1 meeting, 2017. R1-1702719.
31 3GPP. Technical Specification Group Radio Access Network: http://www.3gpp.org/DynaReport/38901.htm, 2022
32 3GPP. Technical Specification Group Radio Access Network: http://www.3gpp.org/DynaReport/38211.htm, 2022
33 R. Nissel: Correctly: IEEE Communications Letters **26** (2022) 2465. https://ieeexplore.ieee.org/document/9825647
34 G. Weijuan and C. Qimei Adaptive coordinated scheduling/beamforming scheme for downlink LTE-advanced system with non-ideal backhaul. 2014 WPMC. https://ieeexplore.ieee.org/document/7014844
35 3GPP. Technical Specification Group Radio Access Network: http://www.3gpp.org/DynaReport/38802.htm, 2017